JOURNAL OF PROPULSION AND POWER
Vol. 25, No. 3, May–June 2009

Pyrolysis/Evaporation Study of Succinic Acid/Polyvinyl Acetate for Reducing Nozzle Erosion

Kenneth K. Kuo,* Ragini Acharya,† Eric Boyd,‡ and Stefan T. Thynell§
Pennsylvania State University, University Park, Pennsylvania 16802

DOI: 10.2514/1.37508

A nozzle boundary-layer control system is under consideration for application in high-pressure rockets to mitigate the erosion rates of a graphite nozzle. The current design contains multiple center-perforated solid grains of fuel-rich materials consisting of succinic acid and polyvinyl acetate. This combination of the fuel-rich grains was selected due to high carbon and hydrogen contents along with relatively low evaporation temperature for generating fuel-rich gases. The characterization of the pyrolysis behavior of fuel-rich grains is a requirement for any subsequent quantitative analysis pertaining to the effect of the nozzle boundary-layer control system on graphite rocket nozzle erosion rates. Two separate experiments were conducted: 1) to determine the regression rate of solid fuel-rich grains under controlled heat flux or temperature conditions, and 2) to characterize its chemical decomposition and/or evaporation behavior. An empirical correlation between heat flux and surface regression rate of fuel-rich grains was developed. From Fourier transform infrared spectroscopy measurements, the fuel-rich grains were found to melt and evaporate at temperatures up to 773 K. These results have been used in parallel study nozzle throat erosion processes using computational simulation.

Nomenclature

k	=	thermal conductivity
L	=	latent heat
$\dot{Q}''$	=	heat flux
$\dot{r}$	=	linear recession rate of solid fuel-rich grain
T	=	temperature
δ	=	thermal penetration depth
ρ	=	density
ϕ	=	porosity

Subscripts

boil	=	boiling
Cu	=	copper
frg	=	fuel-rich grain (succinic acid and polyvinyl acetate)
fus	=	fusion
high$T$	=	high temperature
low$T$	=	low temperature
melt	=	melting
ref	=	reference
s	=	surface
vap	=	vaporization

I. Introduction

GRAPHITE nozzles used in high-pressure nonmetallized solid propellant rocket motors are subjected to thermochemical erosion by hot combustion product gases, which contain several oxidizing species such as H_2O, OH, and CO_2. These oxidizing species can react with graphite by heterogeneous reactions, in particular, at the heated graphite nozzle throat surface. The high heat flux at the nozzle throat results in high surface temperature. This condition facilitates the thermochemical attack on the graphite surface by oxidizing species (such as H_2O, OH, and CO_2). The heterogeneous reactions of these gaseous species with the graphite surface material result in high nozzle throat erosion rates. It has been shown that the erosion rate of the graphite nozzle throat increases almost linearly (pressure exponent between 0.8 and 0.9) with the operating rocket-motor pressure [1]. One of the major approaches for minimizing the erosion rate of the rocket nozzle throat is to control and reduce the surface temperature and oxidizing species concentrations near the upstream region of the throat. This can be accomplished by supplying a secondary flow with relatively low temperature and fuel-rich species near the wall region. A nozzle boundary-layer control system (NBLCS) supplies low-temperature fuel-rich chemical species into the nozzle throat region at a location slightly ahead of the throat station. The temperature of such secondary flow is much lower than the combustion products ($\sim$2800 K) from a rocket motor. The fuel-rich gases can serve as scavengers for oxidizer-rich species produced in the rocket-motor combustor, thereby reducing the erosion rates of the graphite nozzles at high pressures. The NBLCS considered by this research team contains multiple center-perforated grains of ablative materials made of succinic acid (SA) and polyvinyl acetate (PVA) [2]. Succinic acid (with chemical formula $[CH_2COOH]_2$ and chemical name butanedioic acid) has an oxygen balance of -94.84% and polyvinyl acetate (with chemical formula $[CH_2CHCOCH_3]_n$) has an oxygen balance of -181.59%, which means that these materials produce carbon- and hydrogen-rich species upon dissociation or evaporation. The melting points of succinic acid and PVA are 456 and 503 K at 1 atm, respectively; thereby enabling them to melt at very low temperatures. The boiling point of succinic acid at 1 atm is 508 K. It is also a relatively low temperature and is very close to the melting point of succinic acid. Therefore, a mixture of these two components with a large fraction of SA (90% SA and 10% PVA by weight) is considered a suitable fuel-rich material for NBLCS applications. A NBLCS used by Evans et al. [3] in a parallel study showed greater than 95% reduction of the average throat erosion rate from the baseline case without using NBLCS at a rocket-motor operating pressure of $\sim$7 MPa.

Presented as Paper 5775 at the 43rd AIAA/ASME/SAE/ASEE Joint Propulsion Conference and Exhibit, Cincinnati, OH, 8–11 July 2007; received 12 March 2008; accepted for publication 24 September 2008.

*Distinguished Professor, Department of Mechanical and Nuclear Engineering, 140 Research Building East. Fellow AIAA.
†Ph.D. Candidate, Department of Mechanical and Nuclear Engineering, 134 Research Building East. Member AIAA.
‡Graduate Student, Department of Mechanical and Nuclear Engineering, 139 Research Building East.
§Professor, Department of Mechanical and Nuclear Engineering, 326 Reber Building. Associate Fellow AIAA.

The objective of this work is to characterize and analyze the behavior of SA/PVA grains as they are heated to specific surface temperatures or subjected to known heat fluxes, because these data are not available in the literature. Specifically, this work provides the following scientific and technical information:

1) Does the mixture of SA/PVA decompose into smaller molecules when it is heated?

2) If so, at what temperature does it start to decompose?

3) As the surface regresses, how is the instantaneous regression rate related to the energy flux supplied to its surface?

4) Is there a simple mathematical relationship between these two factors?

II. Experimental Approach

A. Conductive Pyrolysis/Evaporation Tests

The regression rate of the SA and PVA mixture was studied using a conductive pyrolysis/evaporation experiment. Samples of the fuel-rich material were prepared from a homogeneous mixture of SA and PVA to create a solid strand that measured 6.35 mm in diameter and 12.7 mm in length. This sample rod was then placed in the conductive pyrolysis/evaporation test setup shown in Fig. 1. The purpose of the experiment is to test the regression rate of the SA/PVA grain over a range of known heat fluxes, while observing its gasification process. This test rig consists of a 10 kW tube furnace, a heated copper slug, and a sample holder inside of a nitrogen purged chamber. The copper slug (rod) was used for its high heat capacity, which enables it to store sufficient thermal energy for maintaining a constant bulk temperature during the test period. The high heat capacity and thermal conductivity of the copper material are favorable for the conductive heat-transfer purpose. The tube furnace heated the copper slug to a desirable initial temperature ranging between 700 and 1163 K. Once the slug reached the desired temperature based upon the measurement of a thermocouple embedded in the copper slug, it was dropped into the guide tube and stopped by a ball valve, so the slug would not generate a high impact force on the test sample. Then the slug was dropped into the test chamber onto the top sample surface by the actuation of a ball valve. A small groove was cut into the top surface of the test sample so that a 25 μm S-type fine-wire thermocouple could be placed at the surface allowing continuous surface temperature measurement during the travel time of the copper slug into the sample.

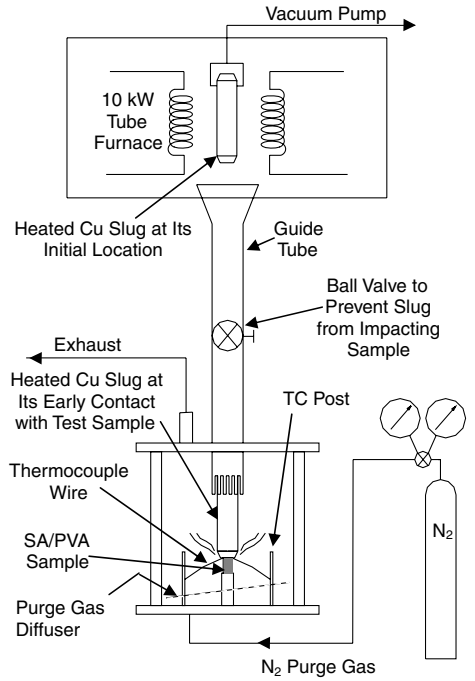

Fig. 1 Schematic diagram of the conductive pyrolysis/evaporation test rig.

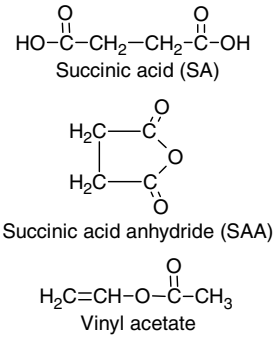

Fig. 2 The structure of succinic acid, succinic acid anhydride, and vinyl acetate.

The chamber was purged by nitrogen at a small flow rate to keep the sidewalls of the test chamber clear for video camera recording. However, due to melting and/or evaporation of the SA/PVA grain with bubble formation at the interface, the surface temperature could not be determined accurately from the fluctuating temperature–time traces. Sample melting was observed at relatively low copper slug temperatures (~700–750 K). At higher temperatures, stronger evaporation from the interface of the SA/PVA test sample and copper slug was also observed. These phenomena are discussed in detail in a later section.

B. Confined Rapid Thermolysis Tests

The confined rapid thermolysis (CRT) behavior of the SA/PVA sample was examined, as well as 99% pure SA acquired from Sigma-Aldrich. In addition, slow thermolysis studies on SA and vinyl acetate (99% pure acquired from Sigma-Aldrich) were conducted for reference purposes. The molecular structures of these compounds and that of succinic acid anhydride are shown in Fig. 2. The objectives of these experiments were to observe and quantify any decomposition of SA/PVA upon rapid heating. The experimental setup was composed of a constant-pressure chamber and a Bruker IFS 66/S Fourier transform infrared (FTIR) spectrometer. In this set of tests, the FTIR results provided conclusive data and mass spectrometry was not required. The technique is very sensitive to decomposition processes occurring in the condensed phase, compared to the gas phase, as the molecules are quenched by the relatively cooler atmosphere into which they evolve. A brief summary of the technique is provided here, because additional details on the experimental procedure are given in [4].

A small amount of the sample, approximately 0.5 mg, was confined between two heated, parallel surfaces within a constant-pressure chamber. The heated surfaces belong to a stationary top heater and a mobile bottom heater, maintained at isothermal conditions by cartridge heaters controlled by proportional–integral–derivative controllers. After the thermolysis chamber was purged by an inert gas, the sample was rapidly heated to the set temperature at heating rates of 2000 K/s. The gaseous products evolving from the condensed phase were sampled by a modulated FTIR beam passing through two ZnSe windows. Thus, the spectra were obtained in near real time with a spectral resolution of 2 cm^{-1} and a temporal resolution of 50 ms. As the two heaters come in contact with the sample, a slight baseline shift in the spectral transmittance was noted and it served as the indicator for the beginning of a heating process.

III. Discussion of Results

A. Results of Confined Rapid Thermolysis Tests

A set of CRT tests was conducted at six different temperatures: 543, 553, 563, 573, 583, and 773 K. At least two tests were conducted at each temperature. We have excluded showing data over the spectral range from 2000 to 2800 cm^{-1}, due to a lack of bands of radiatively absorbing molecules. Figures 3 and 4 show every fifth spectrum from the thermolysis of pure SA conducted at a temperature of 583 K. At this high temperature, the sample quickly melted

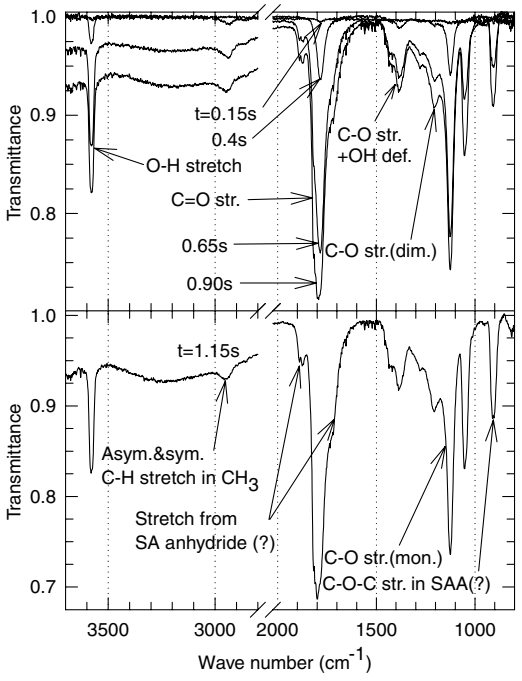

Fig. 3 Spectra from rapid thermolysis of succinic acid at 583 K and 1 atm of N_2.

followed quickly by evaporation. The evolved gases emerged into the probe volume of the FTIR. The spectral features shown in Fig. 3 can be summarized [5] as follows:

1) The O–H stretch near 3580 cm^{-1}: this band evolved at about the same rate as the strong C = O stretch near 1800 cm^{-1}. Later in the event, it decreased faster than the C = O, which suggests that either an SA dimer was formed or that a loss of OH or H-atom abstraction occurred to form water. There was, however, very little water formed, as evidenced by the near absence of the spectral lines close to 1550 cm^{-1}.

2) The asymmetrical and symmetrical C–H stretch in $-CH_3$ near 2900 cm^{-1} are a well-known band for methyl groups, but they were quite weak in the observed spectra.

3) The slope and baseline shift over the spectral range 2800–3500 cm^{-1} occurred since the molecules in the FTIR beam saw cool gases (evaporated SA), and they condensed to form smaller molecules. These smaller molecules produced absorption that is approximately proportional to the wave number. This also occurred for other particles, such as soot.

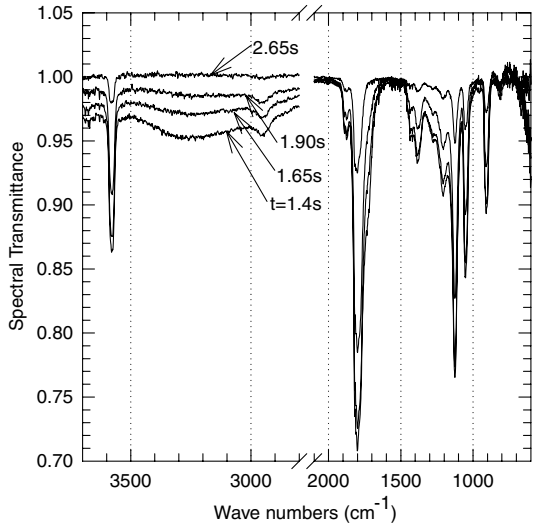

Fig. 4 Spectra from rapid thermolysis of succinic acid at 583 K and 1 atm of N_2.

4) If there was some water formation, it is likely that the succinic acid anhydride (SAA) was formed, and it did not further decompose because temperatures were relatively low in the probe volume of the FTIR. The SAA has strong symmetric and asymmetric bands as indicated in Fig. 3. However, water formation was only detected in relatively small quantities near 1550 cm^{-1}; therefore, the absorption peak at 900 cm^{-1} was most likely not caused by the formation of SAA. Over the spectral range from 1500 to 900 cm^{-1}, there are usually many bands, and often it becomes difficult to interpret the acquired spectral features. There is a possibility of the formation of an SA dimer because the O–H stretch diminished faster than the C = O stretch at a later time as shown in Fig. 4. Thus the band locations were slightly affected. Figure 4 shows that the event was quickly over. That is, the purge gas carried away the evolved gaseous products and particulate matter. The absorption peaks for OH and C = O stretch both decreased as time advances. Similarly, the absorption bands between 1500–900 cm^{-1} also diminished with time.

Figures 5a and 5b show reference spectra obtained from the National Institute of Standards and Technology (NIST) on the vinyl acetate and succinic acid [5,6]. The spectra in Fig. 5c were obtained at the beginning and at the end of the thermolysis event for the SA/PVA sample at a temperature of 563 K. Based simply on these figures, it can be concluded that 1) the SA reference spectra from NIST show that the succinic acid sample with 99% purity contains both the monomer and dimer of SA, and 2) the thermolysis of the SA/PVA sample essentially represents evaporation rather than any noticeable extent of decomposition. If decomposition occurred to any significant extent, CO_2, CO, H_2O, and aldehydes would be detected in the FTIR spectra. The C = O stretch of aldehydes is normally near 1650–1750 cm^{-1} but no aldehydes were detected.

The spectrum at $t = 0.7$ s in Fig. 5c shows the monomer, whereas the spectrum at $t = 6.2$ s in Fig. 5c contains both the monomer and dimer of SA. Figures 6a and 6b show a representative sequence of spectra for the thermolysis of SA/PVA at 563 K. To improve clarity

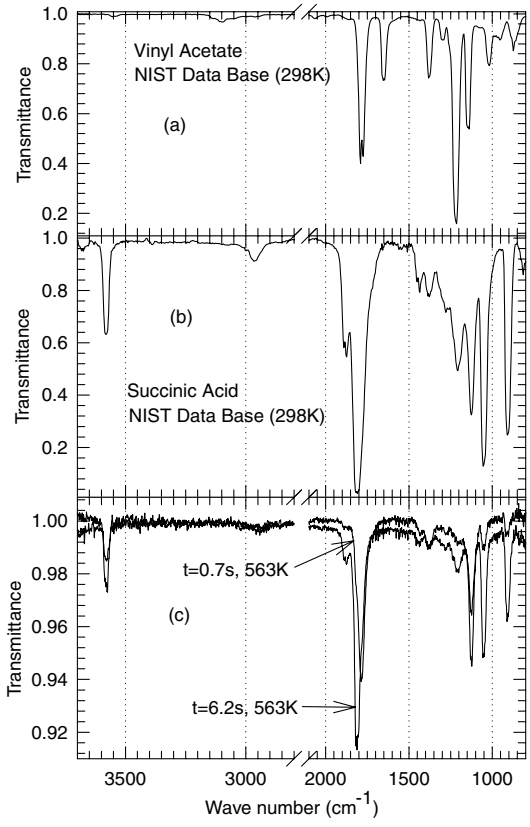

Fig. 5 Comparison of reference spectra from NIST database of succinic acid and vinyl acetate with spectra captured early and late in the thermolysis event of SA/PVA at 563 K and 1 atm of N_2.

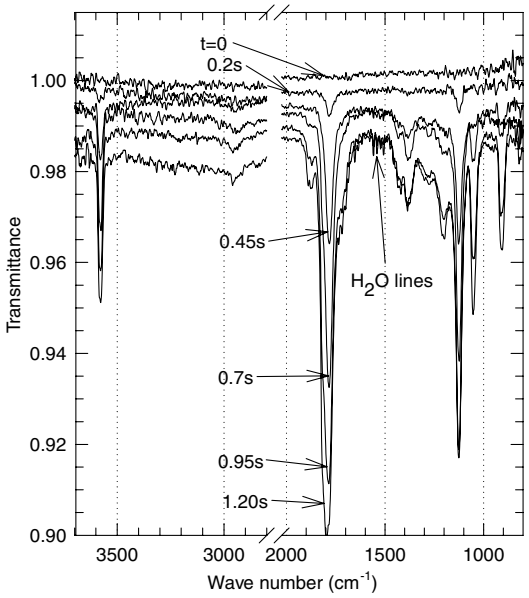

a)

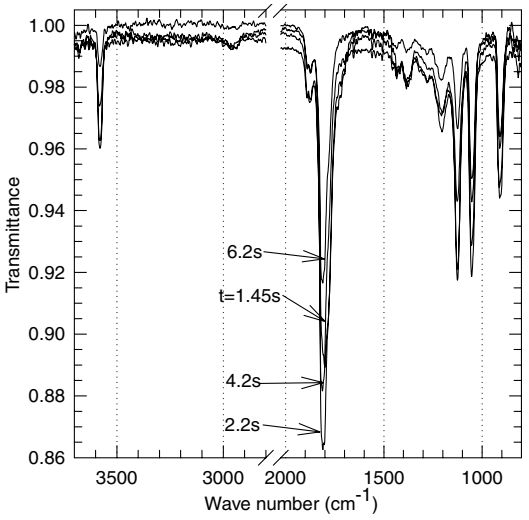

b)

Fig. 6 Spectra from rapid thermolysis of SA/PVA at 563 K and 1 atm of N_2.

of these spectra, they were offset by 0.0025 spectral transmittance units; the data were also deduced using a five-point moving average. All the trends described above for 99% pure SA are present in these spectra.

The SA/PVA sample was also examined at 773 K for using the CRT/FTIR setup. Three tests were performed at this temperature to confirm the findings from relatively lower temperature (543 to 583 K) behavior. To show the results more clearly, an offset of 0.0025 spectral transmittance units and a five-point moving average

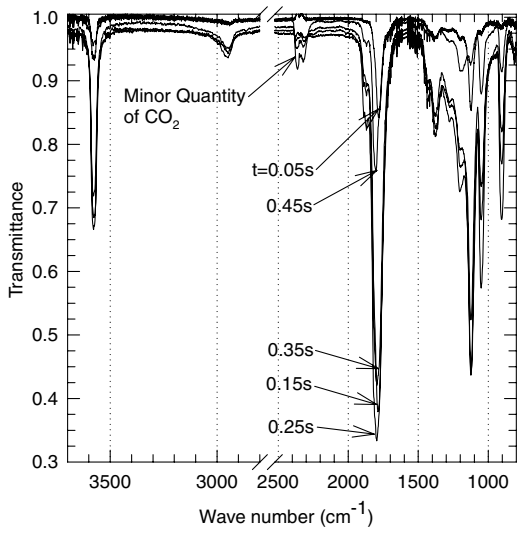

Fig. 7 Spectra from rapid thermolysis of SA/PVA at 773 K and 1 atm of N_2.

were again used for various FTIR spectra files in Fig. 7. From this higher temperature test, the following species and events were observed. The SA monomer evolved first, as it did at the lower temperature tests. Dimer formation occurred later in the event within the probe volume of the FTIR, as opposed to within the confined volume of thermolysis. In addition to a very small amount of formation of water, there was some minor formation of CO_2 and CO. Carbon monoxide is a weakly absorbing molecule, whereas CO_2 is a very strongly absorbing one. The results shown in Fig. 7 were obtained using a larger amount of sample; thus, the extent of absorption is also larger. Because vaporization occurred at relatively low temperatures, the sample departed from the confined volume without any significant extent of decomposition.

B. Regression Rate Measurements

In Table 1, the data from conduction-driven heat-transfer tests show the dependency of the linear surface regression rate of a SA/PVA rod on the copper slug temperature. Table 1 is further divided into three temperature ranges corresponding to different dominant processes involved in the interfacial region. Because of the large thermal inertia of the copper slug, the driving potential for the conductive heat transfer is based upon the temperature difference between the initial slug temperature and the interfacial temperature. The interfacial temperature is governed by the melting or melting with evaporation processes of SA/PVA material. The sample regression rate was deduced from the rate of change of instantaneous interface locations, which was taken from the recorded video images of the SA/PVA test sample. The plot in Fig. 8 shows the displacement of interface location vs time and a curve fit of the data of each test to deduce the overall regression rate at various slug temperatures. As seen from this figure, the linear curve fit for each test is quite suitable and the slope of these curves gives the regression rates under different test conditions.

Table 1 Summary of sample regression rate measurements from conduction-driven heat-transfer tests

Slug temperature, K	Regression rate, mm/s	Temperature range	Dominating mechanism
708	0.725	Low	Melting at interfacial region
748	0.894		
773	0.860	Intermediate	Bubble formation in the melt layer during unstable transition boiling period
813	0.650		
823	0.569	High	Film boiling in the interfacial region with reduced melt layer thickness as temperature increases
923	0.798		
1023	1.120		
1163	1.580		

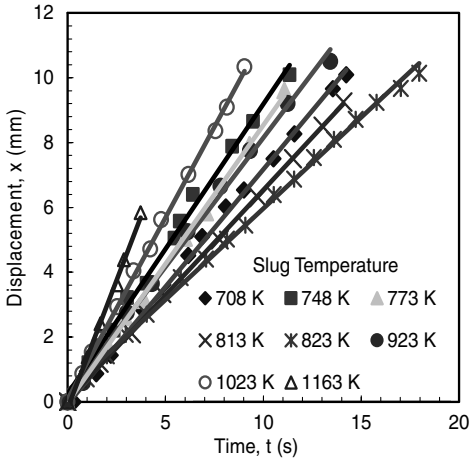

Fig. 8 Recorded instantaneous interface location-time traces of a regressing SA/PVA pellet with a linear curve fit to determine the regression rate from their slopes.

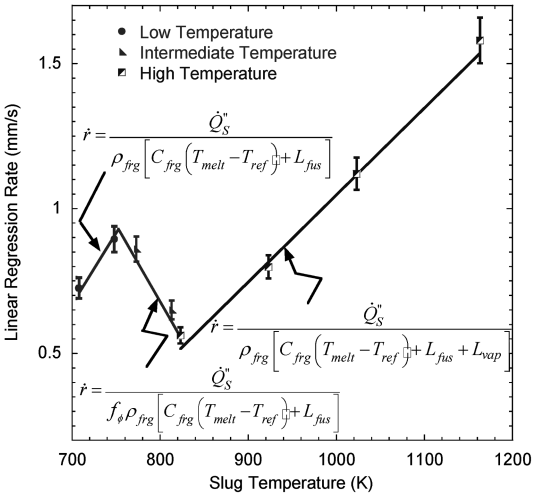

Fig. 9 Measured recession rate variation with the slug temperature for SA/PVA samples.

The linear regression rate with slug temperature is also shown in Fig. 9. As depicted in both Table 1 and Fig. 9, the linear regression rate does not monotonically increase with copper slug temperature. An abrupt change in regression behavior was observed between low-temperature (up to 748 K or 475°C) and high-temperature ranges (823–1163 K or 550–890°C), with the regression rate decreasing considerably in the intermediate-temperature range between 750 and 800 K (or 477–527°C). This change is believed to be due to vaporization of the SA/PVA material following the melting process at higher slug temperature ranges (823–1163 K).

In the intermediate-temperature range (as shown in Fig. 9 and Table 1), the regression rate decreases while the slug temperature increases. This contradicts the general physical intuition. Theoretically, the heat flux available to the SA/PVA test sample should increase with the slug temperature. One explanation for this behavior could be associated with the formation of bubbles in the melt layer. Assuming the melt layer thickness at the end of the low-temperature range to be the same as that in the beginning of the intermediate-temperature range, the bubble formation will hinder the effective heat-transfer rate from the copper slug to the SA/PVA sample because the thermal conductivity of the vapor is much lower than that of liquid in this transition-boiling regime. Therefore, the regression rate decreased with the increase of the slug temperature.

As the slug temperature was further increased, the void fraction in the melt layer due to bubble formation became greater resulting in further decreases in the regression rate. This trend continued up to a slug temperature, which was high enough to result in film boiling of the SA/PVA material. This process resulted in a thinner melting/boiling layer. From this point, the heat flux from the hot copper slug to the SA/PVA sample continuously increased as the slug temperature increased thereby resulting in a monotonic increase of regression rate with slug temperature in the high-temperature range. The dominant mechanism for the three temperature ranges is also explained in Table 1.

Because of the two different phase change processes at low- and high-temperature ranges, two separate relationships were developed between regression rate and slug temperatures. This formulation is described in detail in the following section.

C. Development of Empirical Regression Rate Correlations

As shown in Table 1, the experimental data for the surface regression rate by rapid conductive heating was obtained as a function of the copper slug temperature. It is understood that the heating of SA/PVA grains in the NBLCS of the rocket nozzle is mainly caused by the convective heat-transfer mechanism. Therefore, it is imperative to derive a relationship between the surface regression rate and the heat flux imparted onto the SA/PVA grains. From the above two experiments, it was established that 1) there is only melting and/or evaporation of SA/PVA grains during rapid heating by conductive heat-transfer tests; and 2) the SA/PVA grains do not decompose while subjected to rapid heating, which implies that any decomposition of SA/PVA into fuel-rich gaseous species takes place in the gas phase away from the surface. The latter result is significant for eliminating the consideration of any heterogeneous surface reactions on the SA/PVA grain.

The conductive heat flux from the copper slug to the SA/PVA test sample should be equal to the rate of energy required to either melt and/or evaporate the SA/PVA test sample in the absence of decomposition and/or heterogeneous reactions at the test sample surface. A relationship between the conductive heat flux and the surface regression rate for low- and high-temperature ranges can be obtained through the heat-flux balance at the contact interface between the copper slug and the SA/PVA grain. The mathematical expression for the heat-flux balance at the interface of the copper slug and the fuel-rich grain can be written as follows:

$$\dot{Q}''_S = \begin{cases} \rho_{\text{frg}}[C_{\text{frg}}(T_{\text{melt}} - T_{\text{ref}}) + L_{\text{fus}}]\dot{r} & \text{if } T_s = T_{\text{melt}} \text{ (low-temperature region)} \\ \rho_{\text{frg}}[C_{\text{frg}}(T_{\text{boil}} - T_{\text{ref}}) + L_{\text{fus}} + L_{\text{vap}}]\dot{r} & \text{if } T_s = T_{\text{boil}} \text{ (high-temperature region)} \end{cases} \tag{1}$$

where $\dot{Q}''_S$ is the rate of surface heat flux, ρ_{frg} is the density, C_{frg} is the heat capacity, T_{melt} is the melting temperature, T_{boil} is the boiling temperature, L_{fus} is the latent heat of fusion, L_{vap} is the latent heat of evaporation, and $\dot{r}$ is the linear surface regression rate of the SA/PVA material. Because of the bubble formation in the melt layer for the intermediate-temperature range, the representative surface temperature cannot be expressed directly in terms of T_{melt} and/or T_{boil}. A porosity dependent function f_ϕ must be introduced for this region. Through data analysis, it was found that f_ϕ is dependent on the slug temperature by the following linear relationship given by Eq. (2):

$$f_\phi = 0.0000137 \times T_{\text{slug}}\ [\text{K}] - 9.168 \times 10^{-3} \tag{2}$$

Table 2 Thermodynamic properties of SA/PVA

	SA	PVA
Chemical name/formula	Butanedioic acid ($C_4H_6O_4$)	Polyvinyl acetate, $[\text{-}CH_2CH(OOCCH_3)\text{-}]_n$
Molecular weight, g/mol	118.09	$86 \times n$
λ_{Abl}, W/m · K	0.137	~0.16
ρ_{Abl}, kg/m^3	1560	1190@15°C
C_{Abl}, J/kg · K	1360	1294.24@25°C
$T_{\text{glass transition}}$, K	——	305
T_{melt}, K	493	503
T_{boil}, K	508	——
L_{fus}, J/kg	274,367	——
L_{vap}, J/kg	~374, 000	——

The constants used in Eq. (2) were obtained from regression rate measurement data. The effective heat flux for the intermediate-temperature range can be related to the interfacial heat flux if there was no bubble formation by following Eq. (3). This equation can also be regarded as the mathematical definition of the porosity dependent function f_ϕ:

$$\dot{Q}''_{S_{\text{effective}}} \equiv \frac{\dot{Q}''_{S,\text{with no bubbles}}}{f_\phi} \tag{3}$$

The known thermodynamic properties of both SA and PVA are shown in Table 2. The thermal properties of SA and PVA were used in the determination of the average specific heat of the mixture based on their mass fractions in the mixture, which are required in the calculation of the energy transfer rates at the interface of the SA/PVA sample with the heated copper slug.

In the conductive heating experiments, the rate of surface heat flux is proportional to the temperature gradient at the contact interface, which can be interpreted in terms of slug temperature as shown by Eq. (4):

$$\dot{Q}''_S = k_{Cu}\frac{(T_{Cu} - T_S)}{\delta_{th}} \tag{4}$$

where T_{Cu} is the copper slug temperature, k_{Cu} is the thermal conductivity of copper, δ_{th} is the thermal wave penetration length in the copper slug, and T_S is the temperature at the interface. The surface temperature is equal to the melting temperature of the SA/PVA grain in the low-temperature range and is equal to its boiling temperature in the high-temperature range. Therefore, the linear regression rate of the SA/PVA test sample can be written as a function of the rate of the heat flux at the surface and material properties as given by Eq. (1). To further validate Eq. (1) as a governing equation for the linear regression rate, the following analysis was performed:

1) By assuming that the changes of δ_{th} and k_{Cu} are relatively small from the low-temperature range to the high-temperature range, the ratio of heat-flux rates at these two temperature ranges can be approximated by using Eq. (5):

$$\frac{\dot{Q}''_{S,\text{high }T}}{\dot{Q}''_{S,\text{low }T}} \cong \frac{T_{Cu,\text{high }T} - T_{boil}}{T_{Cu,\text{low }T} - T_{melt}} \tag{5}$$

2) The ratio of regression rates based on the heat-flux balance described by Eq. (1) was calculated and compared with the ratio of measured regression rates. This ratio yields the following relationship given in Eq. (6):

$$\underbrace{\frac{\dot{r}_{\text{high }T}}{\dot{r}_{\text{low }T}}}_{\text{experimental regression rate ratio}} = \underbrace{\left(\frac{\dot{Q}''_{S,\text{high }T}}{\dot{Q}''_{S,\text{low }T}}\right)\left(\frac{C_{frg}(T - T_{ref}) + L_{fus}}{C_{frg}(T_{boil} - T_{ref}) + L_{fus} + L_{vap}}\right)}_{\text{ratio of regression rates based on heat-flux balance (theoretical)}} \tag{6}$$

Using Eq. (5) for the ratio of heat-flux rates in Eq. (6), the following equation was obtained:

$$\frac{\dot{r}_{\text{high }T}}{\dot{r}_{\text{low }T}} \cong \left(\frac{T_{Cu,\text{high }T} - T_{boil}}{T_{Cu,\text{low }T} - T_{melt}}\right)\left(\frac{C_{frg}(T_{melt} - T_{ref}) + L_{fus}}{C_{frg}(T_{boil} - T_{ref}) + L_{fus} + L_{vap}}\right) \tag{7}$$

Comparisons of measured and theoretical ratios determined by Eq. (7) are shown in Table 3. If the above equation is valid, then these two terms should be very close within the measurement errors. The values in the last two columns of Table 3 show that there is good agreement between the experimental data and the theoretical calculated results.

Having established and validated a theoretical relationship between the regression rate and the heat flux, a plot of regression rate versus heat flux was obtained. This plot is shown in Fig. 10. As depicted by the well-represented straight-line fit in this figure, there is a direct linear relationship between the regression rate and the heat flux, irrespective of the slug temperature. This heat flux versus regression rate plot covers all three slug temperature ranges and does not show any abrupt changes in the regression rate behavior as shown in Fig. 9. In this plot, the heat flux was deduced from the relationship given in Eqs. (1–3) and using experimentally measured regression rates.

The empirical correlation for the linear surface regression rate of the SA/PVA material under the known heat flux is given by Eq. (8):

$$\dot{r}\ [\text{mm/s}] = 1.0 \times 10^{-6}\dot{Q}''_S\ [\text{W/m}^2] + 9 \times 10^{-15} \tag{8}$$

The above correlation can be used in the nozzle erosion study with the consideration of NBLCS for mitigation of throat erosion in rocket motors. For example, this correlation is being incorporated in the

Table 3 Comparison of experimental data with theoretical prediction

Low temperature, K	High temperature, K	Heat-flux ratio	Experimental regression rate ratio	Theoretical regression rate ratio
708	823	0.68	1.27	1.18
	923	0.52	0.92	0.89
	1023	0.42	0.65	0.72
	1163	0.33	0.46	0.57
748	823	0.81	1.57	1.40
	923	0.61	1.13	1.06
	1023	0.50	0.80	0.85
	1163	0.39	0.57	0.67

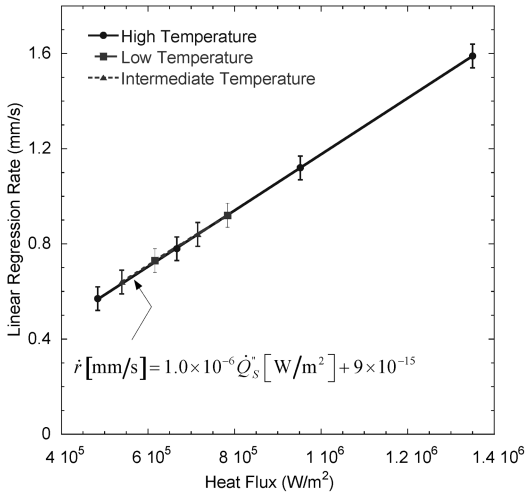

Fig. 10 Empirical correlation between heat flux and surface regression rate for a SA/PVA grain.

graphite nozzle erosion minimization (GNEM) code developed by Acharya and Kuo [2]. An interesting observation was made by the authors in two separate works, in which the SA/PVA grains were used in a rocket-motor simulator test at about 7 MPa [3]. The time calculated for consumption of SA/PVA grains by Acharya and Kuo [2] using correlation developed in the present work coincides with the burning time measured by experiments of Evans et al. [3]. Both calculations and experiments used the same SA/PVA grain configuration (i.e., design, mass, and composition) and found that burning time was close to 2 s. This observation implies that the SA/PVA burning process may not depend on pressure for values up to 7 MPa.

IV. Conclusions

1) From both CRT tests and conduction-driven heat-transfer tests, it was found that the SA/PVA sample does not decompose into smaller molecules for a broad temperature range between 543 and 1163 K. This conclusion was drawn based on the absence of CO_2, CO, H_2O, and aldehydes from the FTIR spectra of gases produced as a result of heating the SA/PVA sample. The SA/PVA sample essentially melts followed by boiling when subjected to intense heating.

2) Even though the regression rate of the SA/PVA sample in the conduction-driven heat-transfer experiments showed three separate slug temperature regions, it was found that the surface regression rate of the SA/PVA sample depends solely upon the surface heat flux by a linear relationship. This correlation developed from this study is necessary empirical input information to the NBLCS analysis for mitigation of the nozzle throat erosion rates.

3) A detailed interpretation of the observed regression rate behavior of the fuel-rich SA/PVA grain was performed based upon the understanding of foam-layer formation, unstable transition boiling, and film boiling processes. The observed abrupt change in the regression rate behavior in the intermediate-temperature region is explained by the bubble formation process.

Acknowledgments

This research investigation was conducted under the sponsorship of the Office of Naval Research (ONR) as a part of the multidisciplinary university research initiative (MURI) project funded under the Contract N00014-04-1-0683. The authors would like to acknowledge the interest, support, and encouragement of Clifford Bedford and Judah Goldwasser of ONR. The input of Jerald Webber, formerly of the Naval Air Warfare Center (NAWC) at China Lake, currently at General Atomics, for the selection of ablative material for NBLCS is highly appreciated. The authors would also like to thank Baoqi Zhang and Eric Boyer for their assistance in making the micro-thermocouples for the interfacial temperature measurements and experimental setup.

References

[1] Acharya, R., and Kuo, K. K., "Effect of Pressure and Propellant Composition on Graphite Nozzle Erosion Rate," *Journal of Propulsion and Power*, Vol. 23, No. 6, 2007, pp. 1242–1254. doi:10.2514/1.24011

[2] Acharya, R., and Kuo, K. K., "Graphite Rocket Nozzle Erosion Rate Reduction by Boundary-Layer Control Using Ablative Materials," AIAA Paper 2007-0782, Jan. 2007.

[3] Evans, B., Kuo, K. K., Ferrara, P. J., Moore, J. D., Kutzler, P., and Boyd, E., "Nozzle Erosion Characterization in a Non-Metallized Solid-Propellant Rocket Motor Simulator," *Advancements in Energetic Materials and Chemical Propulsion* (to be published).

[4] Chowdhury, A., and Thynell, S. T., "Confined Rapid Thermolysis/FTIR/ToF Studies of Imidazolium-Based Ionic Liquids," *Thermochimica Acta*, Vol. 443, No. 2, 2006, pp. 159–172. doi:10.1016/j.tca.2006.01.006

[5] Socrates, G., *Infrared and Raman Characteristic Group Frequencies: Tables and Charts*, 3rd ed., Wiley, Chichester, U.K., 2004.

[6] Stein, S. E., "Infrared Spectra," *NIST Chemistry WebBook, NIST Standard Reference Database No. 69*, edited by P. J. Linstrom and W. G. Mallard, National Institute of Standards and Technology, Gaithersburg, MD, June 2005, http://webbook.nist.gov.

C. Avedisian
Associate Editor